FERMILAB-PUB-09-051-AD

CHARACTERIZATION AND MITIGATION OF COTR SIGNALS FROM A COMPRESSED ELECTRON BEAM*

A.H. Lumpkin, Fermilab, Batavia, IL U.S.A. 60510
N.S. Sereno, W. Berg, M. Borland, Y. Li, and S. Pasky
Argonne National Laboratory, Argonne, IL U.S.A. 60439

Abstract

The Advanced Photon Source (APS) injector complex includes an option for rf photocathode (PC) gun beam injection into the 450-MeV S-band linac. At the 150-MeV point, a 4-dipole chicane was used to compress the micropulse bunch length from a few ps to sub 0.5 ps (FWHM). Noticeable enhancements of the optical transition radiation (OTR) signal sampled after the APS chicane were then observed as has been reported in LCLS injector commissioning. A FIR CTR detector and interferometer were used to monitor the bunch compression process and correlate the appearance of localized spikes of OTR signal (5 to 10 times brighter than adjacent areas) within the beam image footprint. We have done spectral dependency measurements at 375 MeV with a series of band pass filters centered in 50-nm increments from 400 to 700 nm and with an imaging spectrometer and observed a broadband enhancement in these spikes. Mitigation concepts of the observed COTR which has more of a red component than OTR are described.

*Work supported by U.S. Department of Energy, Office of Science, Office of High Energy Physics, under Contract No. DE-AC02-06CH11357.

I. INTRODUCTION

The generation of ultrabright electron beams for various accelerator-based applications often involves compression of a photocathode (PC) rf gun beam using a four-magnet chicane configuration [1,2]. It was recognized via simulations that such beams would be susceptible to microbunching instabilities [3,4] due to coherent synchrotron radiation (CSR) and linac wakefield effects. This was extended to effects of longitudinal space charge (LSC) by Saldin et al. [5], and a suppression scheme for the combined effects on the Linac Coherent Light Source (LCLS) based on a laser heater was proposed several years ago by Huang et al. [6]. However, all of these studies generally targeted microbunching with noticeable gain factors at wavelengths in the FIR at 8 to 12 μm and greater. The gain is exponentially suppressed at shorter wavelengths. There were issues of concern related to beam quality and reduced free-electron laser performance. A second issue became more apparent during the commissioning of the LCLS injector in 2007, when unexpected enhancements of the signals in the visible light optical transition radiation (OTR) monitors occurred after compression in a chicane bunch compressor [7]. These signals were attributed to a LSC-induced microbunching (LSCIM) that started from noise with a concomitant generation of coherent OTR (COTR) at the Al screens [8]. The strong enhancements at random locations and intensities within the beam image footprint precluded OTR-based measurement of beam profiles, emittance, and slice energy spread at LCLS above beam energies of 135 MeV and after the compressor [7].

Since the Advanced Photon Source (APS) injector complex includes a flexible chicane bunch compressor [9] that is similar to that at LCLS, we have an option to use an rf photocathode (PC) gun, and we had experience with SASE-induced microbunching (SIM) [10], a series of experiments was performed to explore the phenomena. We initially performed studies on OTR measured at three screens located after the bunch compressor. We used focus-at-the-object or near-field imaging optics and established that there were clear enhancements of the OTR signals at maximum bunch compression. The compression was monitored with a FIR CTR monitor and interferometer. The shortest bunches generally generate the strongest FIR signals, and the appearance of the enhanced OTR was strongly correlated with the maximum FIR signal, although there appeared to be a slight phase shift between the two maxima. We also accelerated the compressed beam to the end of the linac and evaluated the enhancements at ~375 MeV. The localized spikes in the beam distribution were not only still visible, but even stronger at this energy. At this latter station we have the light transported outside of the tunnel to a small optics lab that allowed us to perform additional spectral dependency measurements. Moreover, the use of a thermionic cathode (TC) gun pulse train with only 40 pC per micropulse was used for comparison purposes when the bunch length was compressed comparably to that of the PC gun beam. Discussions of the possible mechanisms will be presented for the APS case which is similar, but not identical to that of LCLS. A set of mitigation options for the COTR will be described which complement the expected effects of a laser heater [6].

II. EXPERIMENTAL BACKGROUND

The tests were performed at the APS facility which includes an injector complex with two rf thermionic cathode (TC) guns for injecting an S-band linac that typically accelerates the beam to 325 MeV, the particle accumulator ring (PAR), the booster synchrotron that ramps the energy from 0.325 to 7 GeV in 220 ms, a booster-to-storage-ring transport line (BTS), and the 7-GeV storage ring (SR). In addition, there is an rf photocathode (PC) gun that can also be used to inject into the linac as shown schematically in Fig. 1. An extensive diagnostics suite is available in the chicane and after the chicane area as also shown in Fig. 1. The tests were performed in the linac at the three imaging stations (indicated by a flag symbol) after the chicane bunch compressor and at the end of the linac where another beam imaging station is located. A FIR coherent transition radiation (CTR) detector (Golay cell) and Michelson interferometer [11] are located just before the third screen of the three-screen emittance station. A vertical bend dipole and diagnostics screens in this short beamline allow the monitoring of tranverse x-beam size and energy following compression.

The CTR converter is an Al-coated mirror with an 18 mm diameter, and it is mounted with its surface normal at 45 degrees to the beam direction on a pneumatic actuator assembly. A synthetic quartz lens at the port of the cross collimates the beam into the interferometer box. A remotely controlled translation stage steps the position of one arm of the interferometer for the autocorrelation tests. An EPICS interface allows the acquisition of the autocorrelation data. The YAG:Ce and OTR were directed by turning mirrors and relay optics to a Pulnix CCD camera located 0.5 m from the source. These Chicane stations also have options for low- and high-resolution imaging of the beam spot by selecting one of two lens configurations [12].

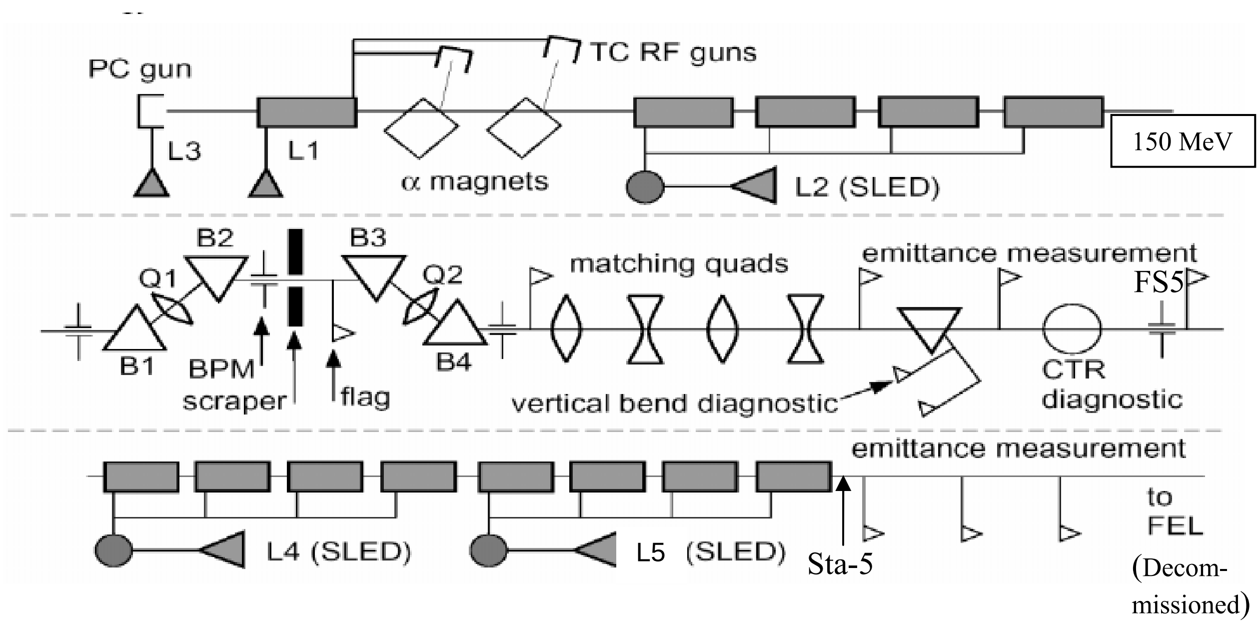

Figure 1: A schematic of the APS linac test area showing the PC gun, the two TC rf guns, the accelerator structures, the chicane, and the diagnostics suite. This includes rf BPMs, beam profile screens (flags), FIR CTR diagnostic, and the vertical bend diagnostic line.

The near-field, low-resolution magnification resulted in calibration factors of 48.8 µm per pixel in x and 38.9 µm per pixel in y. The OTR signal strength with a 400-pC micropulse was too low to use the high-resolution mode with the analog CCD camera. The signal intensity was adjusted with a remotely-controlled iris (with no absolute position readback) in the path to the camera. The OTR and YAG:Ce images were recorded with a Datacube MV200 video digitizer for both online and offline image analyses, and a video switcher was use to select the camera signal for digitizing.

At the end of the linac, the imaging station designated Sta-5 included the optical transport of the visible light out of the tunnel to a small, accessible optics lab where the CCD camera was located. This allowed the access for exploring the spectral dependency of the enhanced OTR. A set of bandpass filters with center wavelengths in 50-nm increments from 400 to 700 nm and 40-nm band width as well as a 500-nm shortpass filter and 500-nm long pass filter were used in the tests. In addition, an imaging spectrometer was installed with options for CCD camera or Pulnix ICCD camera readout. The beam energy was 325-375 MeV at this station. The response functions of these two detector options are somewhat complementary since the CCD chip with a glass cover plate covers about 380 nm to 700 nm with a peak sensitivity at 550 nm, and the GaAs PC of the microchannel plate intensifier has almost constant sensitivity from 525 nm to 880 nm.

Data were also recorded from the electron spectrometer at the end of the linac, but this focal plane converter screen was made of Chromox.

III. INITIAL CTR AND OTR RESULTS

The experiments were initiated by transporting the PC gun beam accelerated to 150 MeV to the chicane area. The rf phase of the L2 accelerator structure located before the chicane was used to establish the appropriate conditions for compression in the chicane. The degree of compression was tracked with the Golay cell signals as shown in Fig. 2. A very strong variation of the FIR signal with L2 phase was observed. There was almost no signal seen when uncompressed, and 300 units seen at the peak compression. The autocorrelation scan was then done and showed a profile width of ~65 μm (FWHM) as seen in Fig. 3. Two separate scans are displayed in the plot. This would mean a round trip time of 130 μm, or about 430 fs (FWHM). The initial drive laser pulse was 3 to 4 ps (FWHM) as determined by an optical autocorrelator.

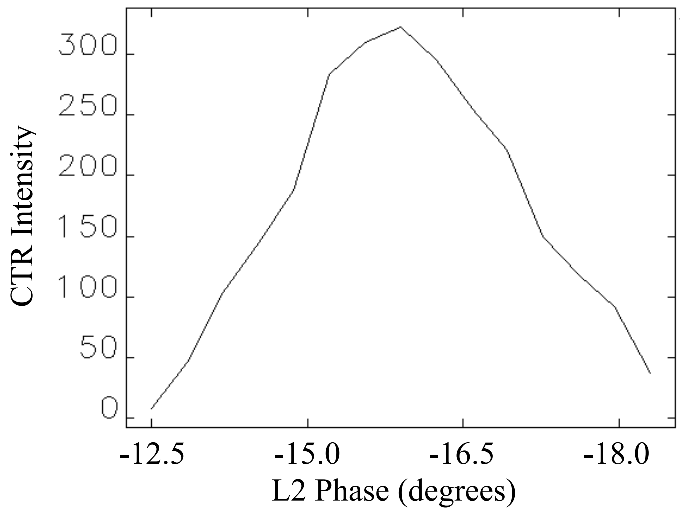

Figure 2: FIR CTR signal from the Golay cell variation with the upstream L2 phase setting. There is some nonlinearity in the conversion of the set points in volts to degrees.

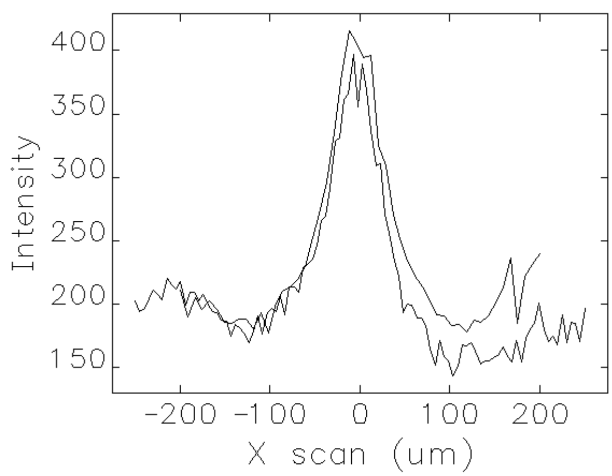

Figure 3: FIR CTR autocorrelation performed after the chicane near maximum compression setup for the PC gun. The two scan profile widths are about 65 μm (FWHM) corresponding to a roundtrip time of 130 μm between the mirrors.

Having determined we had good compression from the Golay-cell data, we then sampled the beam images at the three screens after the chicane in the emittance measurement area. The samples shown are from FS5, the third screen of the set. At the point of minimum compression the OTR image is weak, but visibly tilted in x-y space. No sharp features are seen as shown in Fig. 4. The profile is sampled a little off center of this image, but it is representative of its flatness and low intensity of 15-25 counts. In contrast, the image taken near full compression as indicated by the FIR CTR signal has significantly enhanced localized spikes of about 250 μm (FWHM) extent as shown in Fig. 5. The pseudo-color intensity scale at the right of the image shows that the red areas are high intensity. The profile at the right shows the peak intensity of 180 counts, almost 10 times the adjacent intensities in the beam-image footprint. We do not see the ring-like structure in the enhancement reported at LCLS [7], but we also don't have a harmonic cavity for linearizing longitudinal phase space before the chicane as LCLS has. On this particular run, we noted that there seemed to be a preferred location in the footprint to be enhanced. The enhanced vertical band in Fig. 5 is the same area that shows less enhancement with less compression.

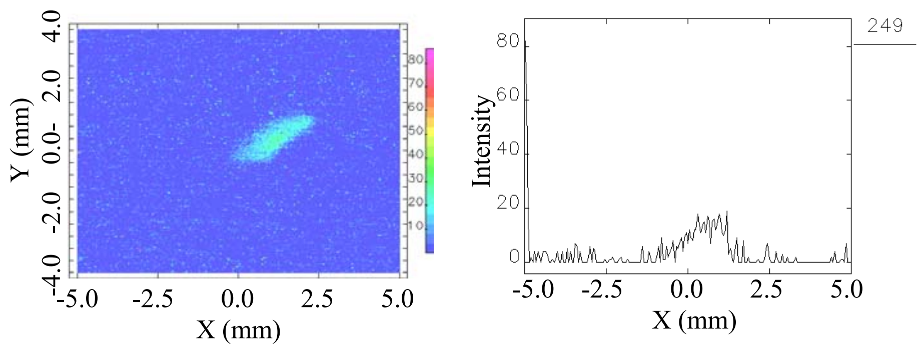

Figure 4: OTR beam image (left) and horizontal profile (right) sampled through distribution after BC with L2 phase = 12 degrees, close to minimum compression.

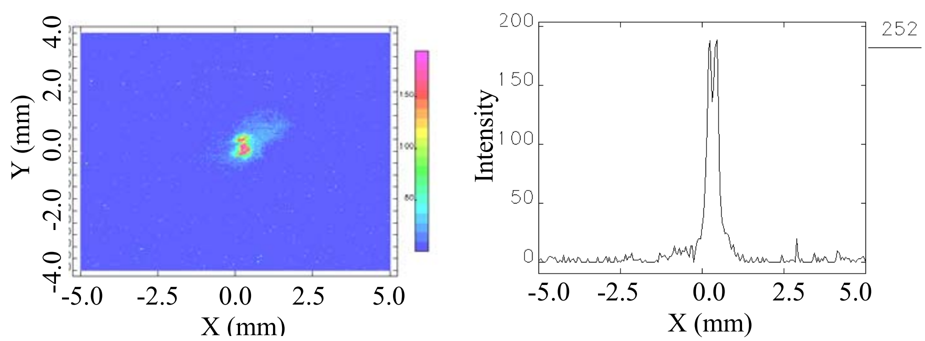

Figure 5: OTR beam image (left) and horizontal profile (right) through a spike in distribution after BC with L2 phase = 14.9 degrees, close to maximum compression.

An additional indication of the effect is shown in Fig. 6, where the peak intensities from the vertical profiles taken though the images at each phase setting show the rapid increase in the enhanced OTR signal in just a few degrees of L2 phase change. An order of magnitude enhancement is clearly seen in this plot. A similar plot for horizontal profiles was done, and this showed a slight shift of the intensity peak compared to the CTR data by 0.4 degrees in L2 phase. Integrated intensities of the ten images at each phase setting do not show the same degree of enhancement. This analysis shows 1.6 to 2 times larger integrated counts at peak compression

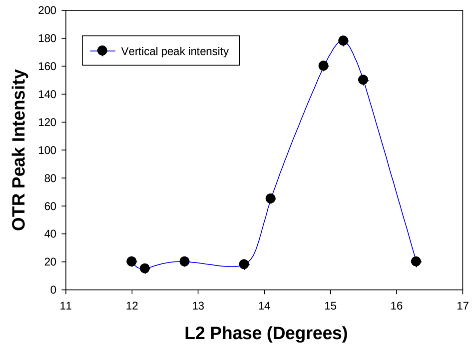

Figure 6: Plot of the peak intensities from the OTR image vertical profiles taken near the enhanced regime coordinates as a function of L2 phase in degrees.

compared to the uncompressed case, with larger fluctuations in the compressed conditions as shown in Fig. 7 (top). The peak intensities on average increase by a factor of 3-4 as shown in the lower plot of Fig. 7. This fact is consistent with the premise that neither variation in charge transport nor CSR-induced clumping of electrons is the cause of these phenomena, but rather that it results from a coherent enhancement of some kind.

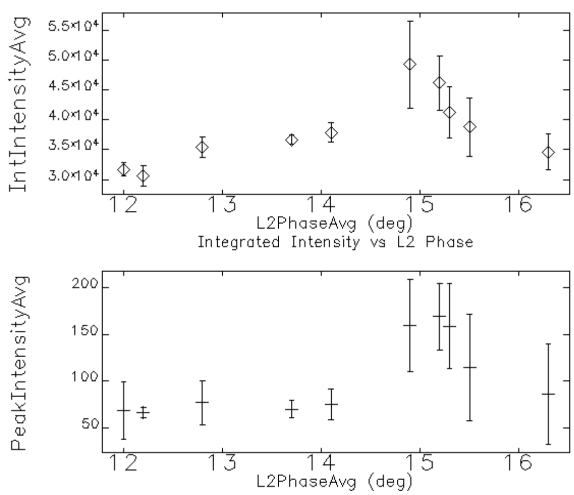

Figure 7: Plot of the OTR image integrals (top) and OTR peak intensities (bottom) using post processing versus L2 phase (degrees). The enhancements occur near the FIR CTR signal maximum.

We accelerated the beam to 375 MeV and imaged the beam spot with OTR at a downstream station, Sta-5. As described previously, this station included transport of the signal outside of the tunnel to a small optics lab. First, we still see enhanced localized spikes when we have compressed the beam as shown in Fig. 8. We also confirmed that these spikes were present at even a compression level corresponding to ½ the peak CTR signal, although their intensity varied more from shot to shot. In Fig. 9 we show the post-processed image intensity integrals (top) and the peak intensities (bottom) versus the L2 phase set point at this location. In this case enhancements of the OTR signals when at maximum compression are about 3-6 times the normal intensity. The strong fluctuations of these enhanced areas are again suggestive of a coherent process, perhaps seeded by noise. (We recall that previously our self-amplified spontaneous emission (SASE) free-electron laser (FEL) experiments indicated preferred hot spots in the spatial distribution of the beam [13].)

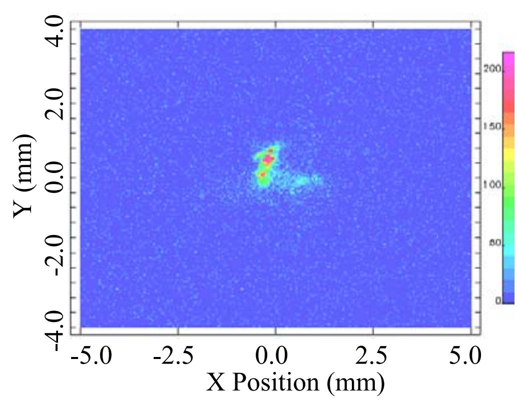

Figure 8: OTR image at 375 MeV showing the enhancements are still present after acceleration beyond the bunch compressor.

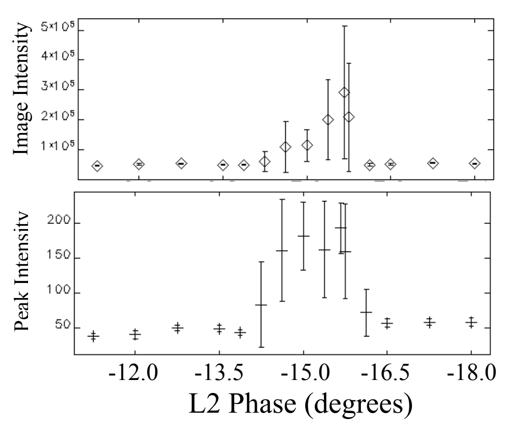

Figure 9: Plot of the OTR image intensity integrals (top) and OTR peak intensities (bottom) at 375 MeV using automated post processing versus L2 phase. The OTR enhancements occur near the same phase as the observed FIR CTR signal maximum.

IV. COTR SPECTRAL EFFECTS

In order to assess the spectral dependency of the OTR enhancements, we accelerated the beam to 325-375 MeV and again imaged the beam spot with OTR at Sta-5. At full compression, we checked the spectral dependency of the enhancements by inserting the bandpass filters in front of the CCD camera. Our preliminary results were that the enhancements were seen at all central wavelengths from 400 to 750 nm (in steps of 50 nm), although relatively weaker in the 400 to 500-nm regime than at 550 nm. We checked the spectral dependence of incoherent OTR from the TC gun beam and saw an intensity roll off in this short wavelength interval which we attributed to the CCD camera response to these different wavelengths. However, this rolloff was not as much as the observed COTR intensity rolloff [14]. In Fig. 10 we show the image intensities normalized for CCD response *and* beam charge. The overall enhancement of the COTR from the PC gun beam is 3 to 4 times the OTR from the TC gun beam, and the COTR has more red enhancements.

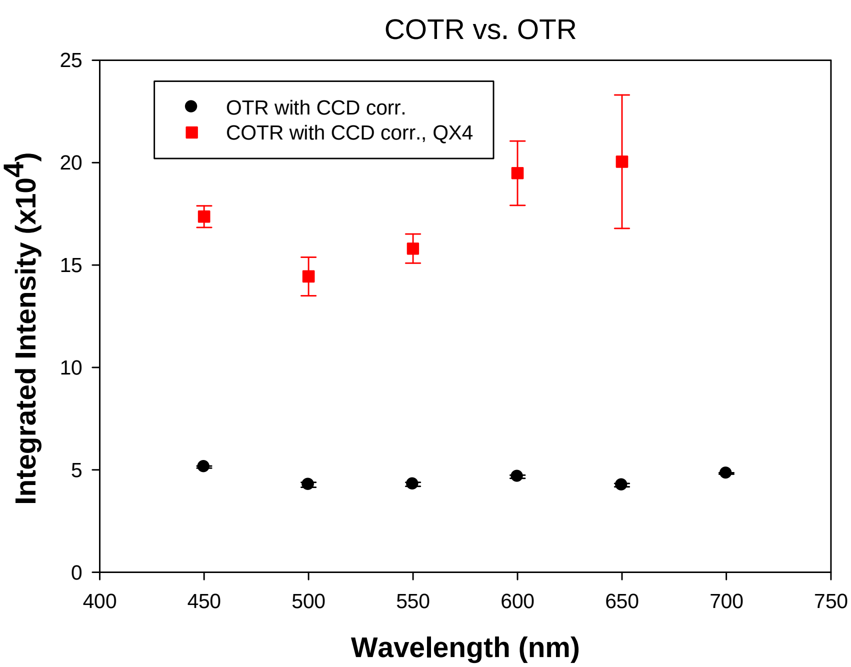

Figure 10: Evaluation of the OTR and COTR image intensities versus the bandpass filter center wavelength for the compressed PC rf gun beam (red squares) and compressed TC rf gun beam (black circles) with charge normalized. The COTR has a relatively stronger red component than the incoherent OTR.

This is corroborated by the spectrometer measurements shown in Fig. 11 where the x-localized emission point for COTR is shown in each image. The scintillators show the full ~2-mm width of the x beam spot, while the COTR source intensity and x locations vary. It is noted that both the YAG:Ce screen and LSO:Ce screen are normal to the beam with an Al mirror behind each at 45 degrees. This mirror is in the same plane as the Al OTR screen when it is inserted. The COTR spectral streak profile is more broadband than the YAG:Ce spectrum which is centered near 530 nm and the LSO:Ce spectrum which is centered near 415 nm as shown in Fig. 11. Such results indicate that this latter scintillator-mirror configuration would still result in COTR spikes in the x-y images. These results support the mitigation scheme described in the next section.

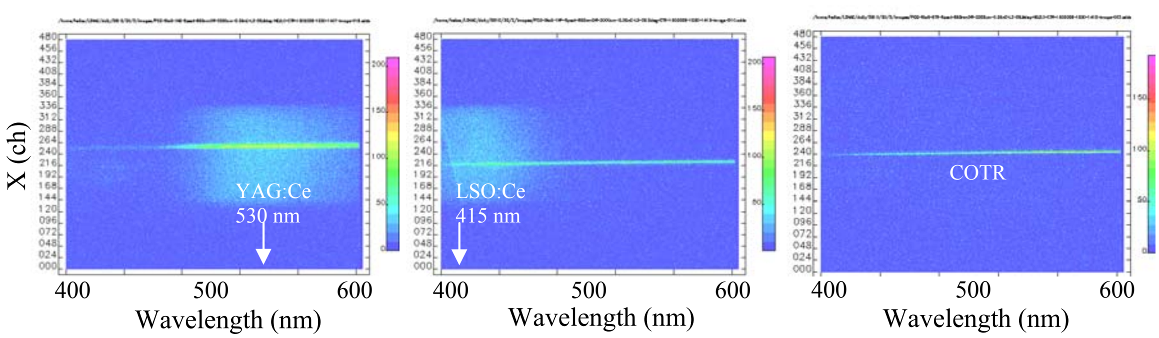

Figure 11: Imaging spectrometer results with CCD camera readout in x-λ space for YAG:Ce plus an Al mirror (left), LSO:Ce plus an Al mirror (middle), and an Al mirror only (right). The localized x extent of the COTR streak in wavelength is evident in all three configurations.

We next extended our spectral studies into the NIR by installing a GaAs PC MCP-intensified CCD camera at the spectrometer output port. This PC has almost constant Q.E. from 525 to 880 nm, and thus complements the spectral response of the bare CCD camera whose sensitivity decreases strongly from 600 to 880 nm. As seen in Fig. 12, the COTR is climbing in intensity almost exponentially from 650 to 880 nm. In this particular run, the compression was adjusted more strongly by increasing the gradient of the L2 rf section, and the autocorrelator gave a 30% narrower width. These are the first spectral data showing the visible and NIR wavelengths together. In this particular pulse and x location the intensity has dropped to a gain factor near 1.0 at 600 nm.

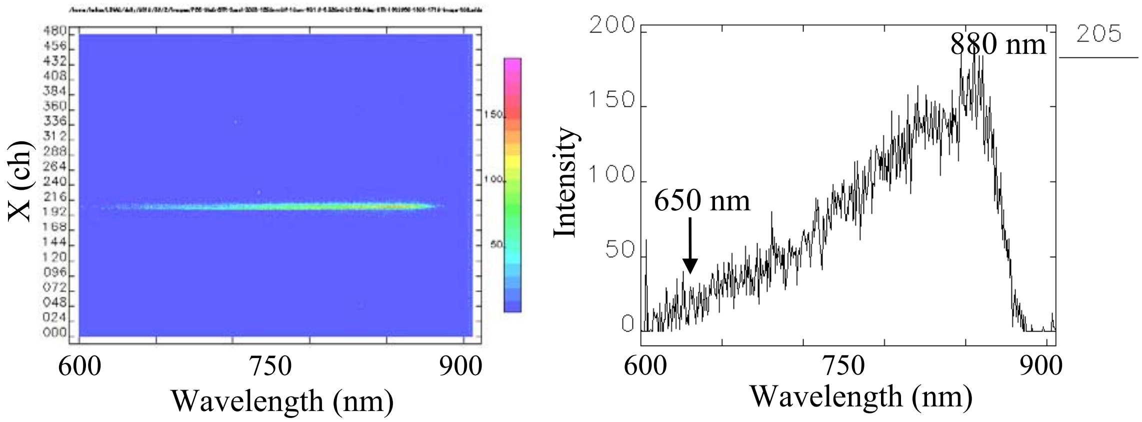

Figure 12: COTR spectrum with NIR MCP utilized showing a) x-λ image and b) profile through the localized x enhancement. The entrance slit was narrowed to give few-nm resolution with grating 4.

V. MITIGATION OF COTR

With the strong evidence of the COTR from the LSCIM being generally more enhanced in the red end of the spectrum at APS and LCLS, we pursued several mitigation concepts. Supported both by the bandpass filter tests and the spectrometer tests at APS, we demonstrated the use of a 400 x 40 nm band pass filter to preferentially transmit the bluish-white incoherent OTR signals while blocking most of the COTR seen in Fig. 13a. With our VICON analog camera we could not image the 0.4-nC beam with the filtered OTR so we also employed the LSO:Ce crystal which has its peak emissions near 415 nm [15] as a means to enhance beam image signal at low charge as seen in Fig. 13b. However, the reported sensitivity of the 12-bit digital camera used at LCLS [16] would have been sufficient for a beam image to be obtained with the filtered OTR and 300 pC of charge.

The LSO:Ce scintillator efficiency is similar to YAG:Ce, but it has a faster response time as indicated in Table 1.

We have evaluated the advantages of the violet end of the spectrum that has generally more OTR than COTR for the LCLS case as shown in Fig. 14. We used a simple model for the $1/\lambda^2$ dependence of the OTR spectral content, and we compared this curve to the COTR estimated by multiplying the OTR intensity by the enhancement/gain factor based on their published model's match to experimental spectral data at LCLS at a screen located after their first chicane [8]. The calculated spectrum for a 3-keV slice energy spread matched reasonably well the time-averaged experimental spectrum reported in that study. We then overlay the CCD camera response on these curves to show which wavelengths were detected. The violet box indicates the 400 x 40 nm BPF regime and graphically shows the COTR mitigation compared to using all of the CCD response regime. The APS COTR case is less violet in hue than the LCLS case so the mitigation should be more complete. We proposed extending the concept by imaging in the ultraviolet (380-200 nm), a regime where the COTR should be relatively even more reduced, i.e. where the gain factor is near 1.0. There is a trade-off, in that standard UV-sensing cameras have reduced sensitivity in the visible regime. However, our present lens transport at Sta-5 does not transmit UV so another experimental setup would be needed. The mitigation options are:

1. Use BPF at 400 nm or short pass filter (SPF) to select preferentially OTR over COTR (x1/100) on most shots at ANL (see Fig. 14).
2. Use BPF centered at 400 or SPF with an LSO:Ce scintillator to image lower charges.
3. Use solar blind or UV filters with UV sensing cameras to use 380 to 200 nm OTR with minimal COTR.

Y (mm)
-2.0 0.0 2.0 4.0

Y (mm)
-2.0 0.0 2.0 4.0

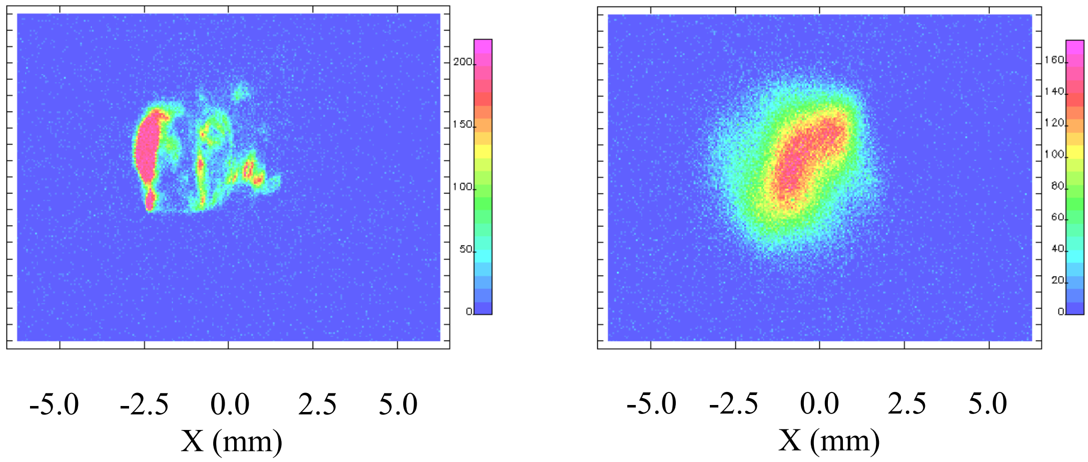

Figure 13: Comparison of beam images at 325 MeV at APS from COTR (left) and with mitigation of COTR (right) using the 400 x 40 nm filter and LSO:Ce crystal.

Table 1: Summary of some radiation converter screen properties for Ce-doped scintillators and an Al OTR screen.

Converter	**Spectrum (FWHM)*, Peak**	**Efficiency**	**Response Time (FWHM)**	**Comment**
YAG:Ce	487-587, 526 nm	1.0*	89 ns*	460 µm Thick
LSO:Ce	380-450, 415 nm	0.46*	40 ns*	530 µm Thick
YAP:Ce	350-400, 369 nm	~0.5	28 ns	460 µm Thick
OTR	Broadband	0.0013*	~10 fs	Surface

*Values from ref. [15].

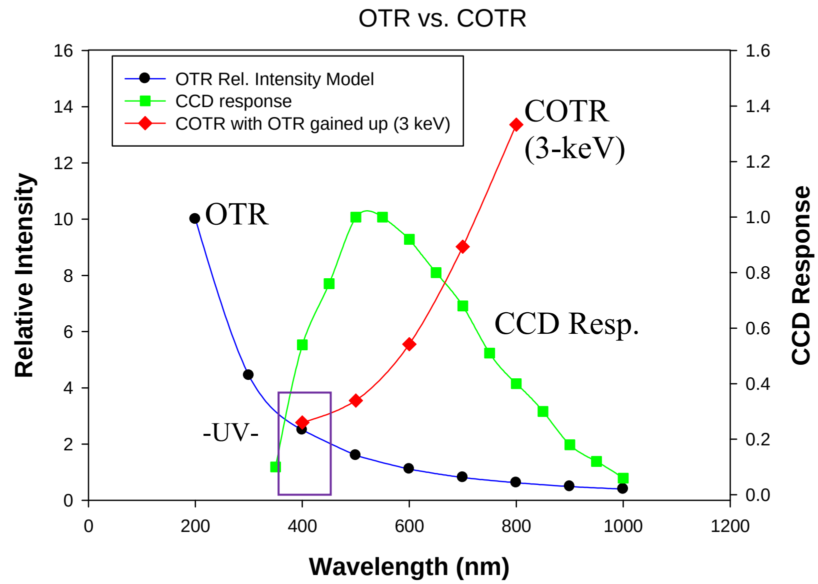

Figure 14: Plots of the nominal OTR intensity dependence on $1/\lambda^2$, the COTR intensity using the calculated gain factor at LCLS for a 3-keV slice energy spread [8], and the nominal CCD camera relative response. The small violet rectangle indicates the 400 x 40 nm BPF regime next to the UV.

VI. CTR AND OTR RESULTS WITH TC RF GUN BEAM

In the course of our studies, we decided to test the effect with the TC rf gun beam. In this case we could generate about 40 pC per micropulse in a macropulse of 25 micropulses that contained about 1 nC total. So the integrated OTR signal should be similar to that of the PC gun beam. We also have no drive laser involved. With the combination of compression in the alpha magnet of the TC gun system and the chicane, we were able to generate an autocorrelation profile width of ~62 μm (FWHM) as shown in Fig. 15. This result is very similar to the PC gun result in Fig. 3, so we have again about a sub-0.5 ps FWHM micropulse at a beam energy now of 150 MeV. The main difference at the chicane is there is now ~10 times less charge in the micropulse compared to the PC gun beam, and 10 times lower peak current. One would expect a significant reduction in any coherent mechanisms. We observed no localized OTR enhancements at the screen after the chicane, nor at the downstream location Sta-5 at the end of the linac. The integrated intensities were the same to about 10% throughout the L2 phase scan. An image from the latter screen under full compression conditions is shown in Fig. 16. We repeated the spectral intensity measurements with the filters and

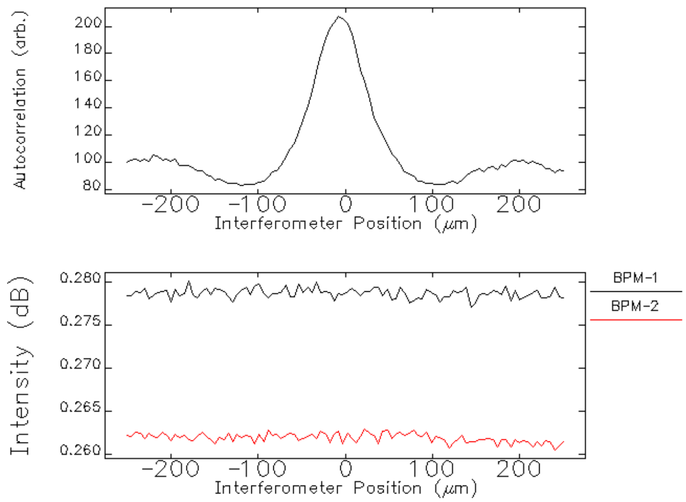

Figure 15: FIR CTR autocorrelation performed after the chicane near maximum compression setup for the TC gun. The scan profile width (top) is about 62 μm (FWHM). The BPM sum signals (bottom) from positions after the chicane were also tracked and show little change during the scan.

determined the nominal overall response of the system to the OTR spectrum and the CCD sensitivity factors as shown in Fig.10.

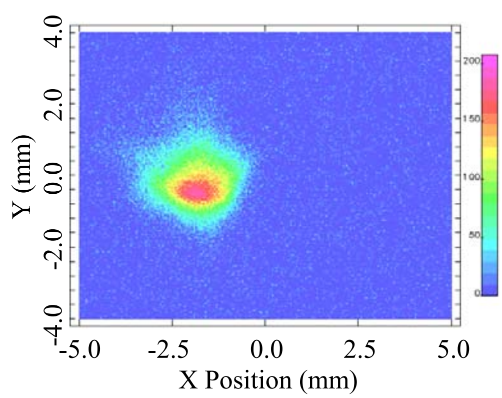

Figure 16: An example OTR image of the TC rf gun beam at the 375-MeV station with maximum compression in the chicane. No localized spatial spikes are evident.

VII. DISCUSSION

We have verified the existence of the enhanced OTR effect after compression at APS and characterized its variation with compression. We accelerated this beam through L4 and L5 and found the enhancement persists and is even stronger. We performed base spectral measurements using bandpass filters and a spectrometer. We also compressed a TC gun beam at much lower micropulse charge (and with a larger energy spread) and observed no resulting COTR. Several characteristics of the enhanced OTR signals may be used to evaluate which mechanism is involved. If we consider electron number constancy, photon number enhancements, intensity fluctuations, charge dependence, and spectral structure observed, we may be able to discriminate among LSC microbunching, a longitudinal spike, multiple sub-micron spikes, and CSR-induced clumping. We initially wondered whether there were microbunching from the drive laser interaction with the low-energy photoelectrons such as found under high laser power conditions [17], but a simple calculation of the laser field strengths showed this effect would not be measurable. Since we measured and accepted that the transported charge through the chicane was basically constant to 10 % during the phase scan, we cannot explain the large photon number enhancements as only due to CSR-induced clumping of the charge distribution. Both our preliminary spectral sampling across the visible light region with band pass filters of 40-nm band widths and an imaging spectrometer showed a broadband character like that of incoherent OTR, but COTR had a relatively much stronger red component. Our broadband visible spectrometer data are consistent with coherent enhancements of wavelengths longer than a fine longitudinal structure, such as a leading-edge spike or multiple fine spikes, but in addition they are consistent with the broadband LSCIM based spectra. We have reported separately that we have found a connection with the localized enhancements seen in our old SASE-related COTR data at 530 nm and with the apparent LSCIM beam structures entering the undulators [13]. The localized spatial spikes of COTR are nominally consistent in transverse size with the coherence length of ~1.5 $\gamma\lambda/2\pi$ for visible wavelengths such as discussed by

Venturini [18]. There is also now clear evidence from the laser heater tests at LCLS that the visible light COTR is strongly damped when the slice energy spread is purposely increased, as expected [19]. These latter two aspects support the LSCIM interpretation for the COTR after the APS compressor which is similar in design to LCLS's.

VIII. SUMMARY

In summary, we have initiated investigations on the enhancement of OTR signals in the visible light regime following bunch compression of our PC rf gun beam at APS. Although the enhancements are not as high as that reported at LCLS [7,8], we do see order of magnitude signal increases in localized spatial spikes within the images after the chicane and two orders of magnitude enhancements at the end of the linac. At this time the coherent enhancement appears consistent with many fine sub-micron spikes or LSCIM at visible wavelengths after bunch compression. The practical effect is that one cannot simply evaluate emittance of the beam for different compressions using the OTR screen images. One normally uses the YAG:Ce screens at APS for signal considerations, and LSO:Ce screens are now an option to consider. We did not see the effects in the TC gun beam when it was compressed similarly; since this involved equally short electron pulses but only 40 pC per micropulse, it lends support to the conclusion that the enhancement is driven by a coherence phenomenon. We have clearly established the COTR trend toward higher intensities at the red end of the visible spectrum and into the NIR so that mitigation schemes based on imaging the violet and ultraviolet end of OTR are appropriate at APS and LCLS, and similar accelerator configurations. The growing interest in these COTR effects is indicated by the time allowed for discussion in the recent microbunching instability workshop [20].

IX. ACKNOWLEDGEMENTS

The authors acknowledge support from M. Wendt of Fermilab and R. Gerig, K.-J. Kim, and H. Weerts of the Argonne Accelerator Institute. They acknowledge S. Shoaf (ANL) for controls support and K. Nemeth (ANL) for estimating the laser-electron interaction. They also acknowledge discussions on COTR with D. Dowell, H. Loos, J. Frisch, and Z. Huang of LCLS and with R. Fiorito of the Univ. of Maryland and D. Rule of NSWC.

REFERENCES

[1] S.V. Milton et al., Science **292**, 2037 (2001).

[2] Linac Coherent Light Source (LCLS) Conceptual Design Report, SLAC Report No. SLAC-R-593(2002).

[3] M. Borland et al., Proc. 2001 PAC, 2707-2709 (2001); M. Borland et al., Nucl. Instr. Methods Phys. Res. Sect. A **483**, 268 (2002).

[4] E.L. Saldin, E.A. Schneidmiller, and M.V. Yurkov, Nucl. Instr. Methods Phys. Res. Sect. A **490**, 1 (2002).

[5] E.L. Saldin, E.A. Schneidmiller, and M.V. Yurkov, DESY Report No. TESLA-FEL-2003-02, 2003.

[6] Z. Huang et al., PRST-AB **7**, 074401 (2004).

[7] D.H. Dowell et al., “LCLS Injector Commissioning Results”, Proc. of FEL07, Aug. 26-30, 2007, Novosibirsk; R. Akre et al., Phys.Rev.ST-AB **11**, 030703 (2008).

[8] D. Ratner, A. Chao, and Z. Huang, “Three-Dimensional Analysis of Longitudinal Space Charge Microbunching Starting from Shot Noise”, submitted to the Proc. of FEL08, Gyeongju, Korea, Aug. 24-29, 2008.

[9] M. Borland, Phys. Rev. ST-Accel. Beams **4**,074201 (2001).

[10] A.H. Lumpkin et al., “First Observation of z-dependent Microbunching using Coherent Transition Radiation,” Phys. Rev. Lett., Vol. 86(1), 79, January 1, 2001.

[11] A.H. Lumpkin et al., "Initial measurements of CSR from a Bunch-Compressed Beam at APS." Proc. of FEL05, JACoW/eConf C0508213, 608 (2005).

[12] B.Yang et al., "Design and Upgrade of a Compact Imaging System for the APS Linac Bunch Compressor", BIW2002, AIP Conf. Proc. 648, 393 (2002).

[13] A.H. Lumpkin, R.J. Dejus, and N.S. Sereno, "COTR and SASE Generated by Compressed Electron Beams", submitted to the Proc. of FEL08, Kyeongju Korea, August 26-30, 2008.

[14] A.H. Lumpkin, N. S. Sereno, W.J.Berg, M. Borland, Y. Li, and S. Pasky, "Spectral and Charge-Dependence Aspects of Enhanced OTR Signals from a Compressed Electron Beam", submitted to the Proceedings of LINAC08, Sept. 28-Oct. 3, 2008, Victoria, Canada.

[15] W.J. Berg, A.H. Lumpkin, and B.X. Yang, "Characterization of Ce-Doped Scintillating Crystals for Imaging Electron Beams at the APS Linac", Proc. of the XX International Linac Conference, Monterey, CA, 158 (2000).

[16] H. Loos, (private communication) December 2008.

[17] Karoly Nemeth et al., PRL 100, 095002 (2008).

[18] M. Venturini, "Nonlinear Correction to the Gain of the Microbunching Instability", Proc. of the Microbunching II Workshop, Berkeley CA, Oct. 6-8, 2008.

[19] P. Emma, (private communication) December 2008.

[20] Agenda for Microbunching Instability Workshop II, Chairman W.M. Fawley, LBNL, Berkeley CA, October 6-8, 2008.